ChemPubSoc Europe

DOI: 10.1002/cphc.201300711

The Lateral and Axial Localization Uncertainty in Super-Resolution Light Microscopy

Bernd Rieger and Sjoerd Stallinga*[a]

A study of the uncertainty of localizing single-molecule emitters for super-resolution light microscopy is presented. Maximum likelihood estimation (MLE) is found to be superior to least-squares fitting for low background levels, but the performance difference between the two methods decreases to a few percent for practical background levels. It is shown that the performance limit of MLE, the Cramér–Rao lower bound, is well described by a concise analytical formula with only spot width and signal and background photon count as input parameters. These predictions for the lateral localization uncertainty are compared with the localization error obtained from repeated localizations of the same single-molecule emitter. Agreement within a few percent is found, thus verifying the validity of the fitting model and the concise analytical approximation. The analysis is extended by novel analytical results for the dependence of the axial localization uncertainty on background level for the astigmatic, bifocal, and double-helix methods.

1. Introduction

The family of localization microscopy techniques, which comprise (F)PALM,[1,2] STORM,[3] GSDIM,[4] and dSTORM,[5] relies on localizing stochastically activated fluorescent single molecules for obtaining a resolution in light microscopy far below the conventional diffraction limit. A time series of image frames of randomly different sparse subsets of all emitters is acquired and analyzed for determining the position of all emitters that have been activated in the course of the time of the experiment, thereby assembling a super-resolution light microscopy image of the sample. The key process in analyzing the images is the localization of single emitters found in the raw frames. A first step in this process is finding the different regions of interest (ROIs) containing the candidate emitter images. These ROIs are typically three times larger than the image spot. A second step is to extract the position of the emitter from the ROI image by a fitting algorithm. Two different computational algorithms are in common use: the least squares (LS) algorithm and the maximum likelihood estimation (MLE) algorithm.

Both the LS and MLE methods work with a model for the expected number of photons μ_k at pixel k within each ROI, which is fitted to the measured number of photons n_k. Fitting the model to the data is done by means of maximizing a function, the logarithm of the likelihood that the model fits the data given a probabilistic process (noise model). In the case of Gaussian noise with uniform variance V we find the LS function [Eq. (1)]:

$$W_{\mathrm{LS}} = -\sum_k \frac{(n_k-\mu_k)^2}{2V} \tag{1}$$

and in the case of shot noise we find the MLE function [Eq. (2)]:

$$W_{\mathrm{MLE}} = \sum_k [n_k log\mu_k - \mu_k - log(n_k!)] \tag{2}$$

In addition, a model for the expected number of photons per pixel μ_k as a function of the fit parameters is needed. This number is found by integrating the point spread function (PSF) over the $a\times a$ pixel area; usually a Gaussian plus constant background will do fine as model PSF [Eq. (3)]:[6]

$$H = \frac{N}{2\pi\sigma^2} e^{-\frac{(x-x_0)^2+(y-y_0)^2}{2\sigma^2}} + \frac{b}{a^2} \tag{3}$$

with as fitting parameters the lateral coordinates of the emitter (x_0,y_0), the signal photon count N, the spot width σ, and the number of background photons per pixel b. The LS or MLE function can be optimized with various numerical methods, such as the Levenberg–Marquardt method. Both models give viable results and are used in practice.

Both methods have different performance limits. Thompson, Larson, and Webb (TLW)[7] have proposed an expression for the best possible localization uncertainty for the LS method (or "Gaussian mask estimator" as they call it). This limit, with a small correction due to Mortensen et al.,[8] is given by [Eq. (4)]:

$$\Delta x|^2_{\mathrm{LS}} = \frac{\sigma^2 + a^2/12}{N}\left(\frac{16}{9} + 4\tau\right) \tag{4}$$

[a] Dr. B. Rieger, Dr. S. Stallinga
Quantitative Imaging Group
Delft University of Technology
Lorentzweg 1, 2628CJ Delft (The Netherlands)
E-mail: s.stallinga@tudelft.nl

Supporting Information for this article is available on the WWW under http://dx.doi.org/10.1002/cphc.201300711.

with τ roughly equal to the ratio between the background intensity b/a^2 and the peak signal intensity $N/2\pi\sigma^2$ [Eq. (5)]:

$$\tau = \frac{2\pi b(\sigma^2 + a^2/12)}{Na^2} \tag{5}$$

The correction of Mortensen et al. pertains to the factor "16/9" within the brackets, which replaces the original factor "1" of the TLW formula. The performance limit of the MLE method corresponds to the Cramér–Rao lower bound (CRLB), the best possible variance of an unbiased estimator.[9,10] According to Mortensen et al.,[8] the CRLB is given by [Eq. (6)]:

$$\Delta x|^2_{\mathrm{MLE}} = \frac{\sigma^2 + a^2/12}{N}\left(1 - \tau\int_0^\infty dt\,\frac{t}{1+\tau e^t}\right)^{-1} \tag{6}$$

We have shown previously that this exact but nonanalytical result can be approximated excellently by a concise analytical formula [Eq. (7)]:[11]

$$\Delta x|^2_{\mathrm{MLE}} = \frac{\sigma^2 + a^2/12}{N}\left(1 + 4\tau + \sqrt{\frac{2\tau}{1+4\tau}}\right) \tag{7}$$

This formula can be derived heuristically as follows. The factor between brackets in Equation (6) is equal to 1 for $\tau = 0$ and scales as $1/4\tau$ for $\tau \gg 1$. Interpolation between these two limiting cases then gives a variance of the localization error proportional to $1+4\tau$. The residual error between the exact result from Equation (6) and the interpolation $1+4\tau$ appears to be a function that qualitatively behaves as approximately $\sqrt{\tau}$ for small τ and levels off to a constant value for large τ. The third term between brackets in Equation (7) describes this residual rather well. Similar formulas can be obtained for the CRLB for the spot width σ and the signal photon count N (see the Supporting Information for a derivation) [Eqs. (8) and (9)]:

$$\Delta\sigma|^2_{\mathrm{MLE}} = \frac{\sigma^2}{4N}\left(1 + 8\tau + \sqrt{\frac{8\tau}{1+2\tau}}\right) \tag{8}$$

$$\Delta N|^2_{\mathrm{MLE}} = N\left(1 + 4\tau + \sqrt{\frac{\tau}{14(1+2\tau)}}\right) \tag{9}$$

Figure 1 shows the background dependence of the uncertainties as well as the relative error of the analytical approximations as a function of the dimensionless background parameter τ (less than 2% for x_0 and y_0, 2% for σ, and 0.5% for N).

MLE fitting follows the CRLB [effectively Eq. (7)] for a wide range of signal and background photon counts.[11,12] The MLE method is always superior to the LS method. The performance difference between the two methods, however, decreases for increasing background levels. The reason is that the difference between the noise variance for pixels away from the spot peak approximately $\sqrt{b}$ and the pixel at the spot peak approximately $\sqrt{b(1+\tau^{-1})}$ gets small in the case for which the signal-to-background ratio decreases. Approximating the likelihood with a noise model with a uniform noise variance then becomes a viable approach. Figure 2 shows simulation results to corroborate the given performance limits. The simulation results of Figure 2 are largely the same as described in ref. [11]. MLE is indeed superior to LS, but for large values of the background level b/N they are very close.

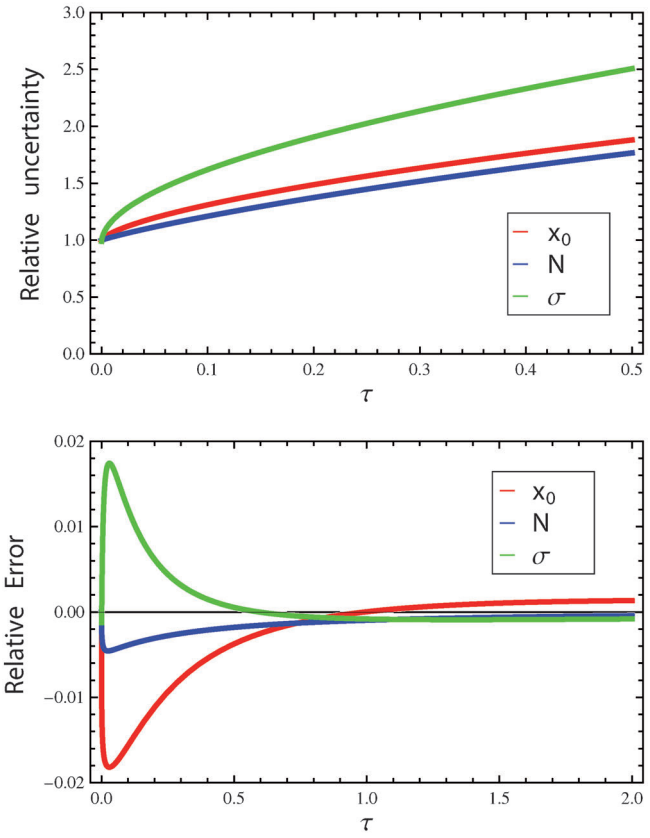

Figure 1. Dependence of the uncertainty in estimating the emitter position, the signal photon count, and the width of the fitted Gaussian PSF relative to the zero background uncertainties as a function of the scaled background parameter τ (top) and the relative error of the approximations for the uncertainties [Eqs. (7)–(9)] as a function of the scaled background parameter τ (bottom).

The predicted localization uncertainty can be compared to the experimental localization uncertainty obtained from repeated localizations of the same emitter. Such a comparison can be made by measurements on sparsely labeled control slides or by hand-picking clusters of localizations from a localization microscopy data acquisition originating from isolated single molecules.[13] The MLE prediction for the localization uncertainty has been found in good agreement with data obtained from such control slides[12] but no comparison with real localization microscopy data acquisitions has been made so far.

There are three different methods for measuring the axial position of single emitters that are often used in practice. The astigmatic focusing method[14] uses a cylindrical lens for producing elongated spots; the aspect ratio of the elliptical spot shape is a measure of the z-position of the emitter. The bifocal or biplane method[15] splits the spot in two mutually defocused subspots imaged on two detector halves; the spot size ratio is now measuring the z-position. The double-helix method[16,17]

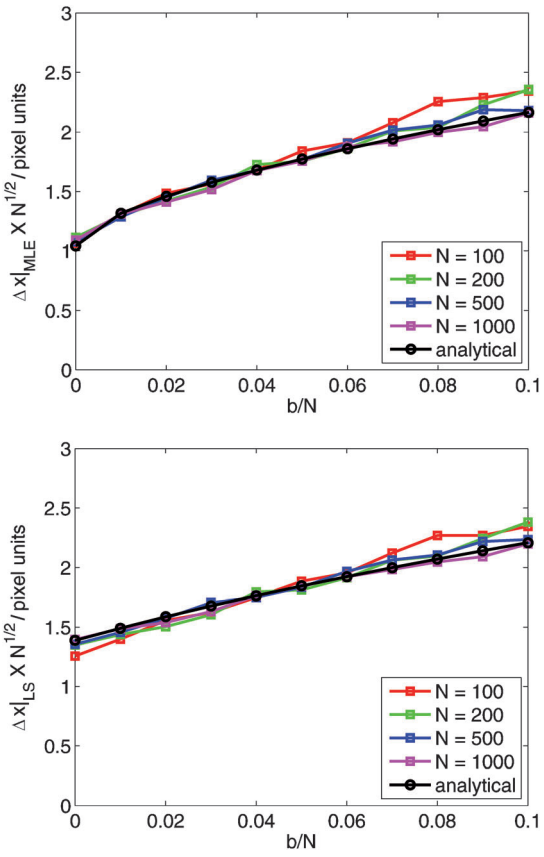

Figure 2. Simulation results for the localization uncertainty scaled with $\sqrt{N}$ for the MLE method (top) and LS method (bottom) as a function of relative background level b/N for different signal photon counts N and the scaled localization uncertainty according to Equation (7) for MLE and Equation (4) for LS, which show the validity of these performance limits. Simulations are based on PSFs calculated with vectorial high-numerical-aperture (NA) theory (assuming water immersion at NA = 1.25 and wavelength $\lambda = 500$ nm) for point emitters with randomized position on a grid of 9×9 pixels with pixel size $a = 100$ nm in object space (corresponding to Nyquist sampling), and are fitted with a MLE algorithm using a Levenberg–Marquardt optimizer. All data points are averages over 1000 randomized spot realizations.

splits the spot into two adjacent subspots, such that the relative orientation of the subspots measures the z-position. Interestingly, the first two methods seem to be a rediscovery of methods that have been in common use in the field of optical data storage for decades.[18–20] The CRLB for the spot width in the two lateral directions (astigmatic method), for the two defocused spots (for the bifocal method), or the relative orientation of the two subspots (for the double-helix method) can be analyzed with PSF models similar to the standard Gaussian PSF model, and in turn these CRLB values lead to performance limits for the axial localization.[21–24]

Herein, we address three issues concerning the MLE methodology. First, we discuss the effects of so-called excess noise of electron-multiplying charge-coupled devices (EM-CCDs). Second, we show how the lateral localization uncertainty can be measured directly and efficiently from standard localization microscopy datasets and how it compares to the predictions of MLE fitting. Third, we present semiexact formulas for the axial localization uncertainty as a function of the background level similar to the result of Equation (7) for the lateral localization uncertainty.

2. Results and Discussion

2.1. Excess Noise

Images acquired with an EM-CCD use an avalanche electron multiplication process during readout. The electron multiplication process effectively drowns the readout noise but introduces an additional noise source, excess noise.[25] Theory suggests that this excess noise effectively doubles the noise variance making the localization uncertainty a factor of $\sqrt{2}$ worse.[8,26] This effect of excess noise, however, is indistinguishable from an underestimation of the photon count with a factor of two, because of the way in which the camera gain g is calibrated. The measured number of photons is calculated from the measured signal by dividing the latter by the gain g. Usually the gain g (and the readout noise variance V) is measured from the linear relation $\mathrm{var}(I) = g \times \mathrm{mean}(I) + V$ between the variance and the mean of the measured signal based on the assumption that there is only shot noise and readout noise.[27] In the case of an EM-CCD the readout noise is absent ($V = 0$) but the excess noise doubles the shot noise variance, so that the gain is overestimated by a factor of two. As a consequence, the measured number of photons is underestimated by a factor of two. The effect would then be that the localization uncertainty is a factor $\sqrt{2}$ higher than it would be with the correct photon count and having shot noise only. A better camera calibration procedure for measuring the photon count from the detector signal would thus be desirable.

2.2. Lateral Localization Uncertainty

In localization microscopy image acquisition each emitter switches between an "off" state and an "on" state. The switching between these states may be described as a first-order process characterized by timescales t_{on} and t_{off}. The frame time of the camera t_{frame} is often somewhat smaller than the on-time t_{on} so that each activation event lasts typically a few camera frames. The N_{raw} localizations fitted from the ROIs in all the individual camera frames can be condensed into $N < N_{raw}$ localization events by grouping spatially nearby localizations (distance less than three times the sum of the localization uncertainty of the two to-be-merged localization events) in consecutive frames into single localization events. The underlying assumption is that all frames are images of sparsely distributed active emitters, thus making it likely that localizations obtained from subsequent camera frames that are spatially close to each other, are in fact originating from the same active emitter. This procedure improves the localization uncertainty, as the average number of photons per localization event now scales with the fluorescent on-time t_{on} rather than with the frame time t_{frame}. The best estimation of the emitter position from a sequence of M localizations is found from the average of the individual localizations, weighted with the inverse of the localization variances found from the individual fits. These localiza-

tion variances are obtained from evaluating the Fisher information matrix for the set of model parameters (emitter position, spot width, signal photon count, background) for which the likelihood function was optimal, and taking the diagonal elements of the inverse of this Fisher matrix (the CRLB values).

The grouping procedure has an unexpected but desirable byproduct. We now have a series of independent measurements of the positions of many emitters. The variance of the distribution of localizations that are grouped into a single localization event is a direct experimental measure for the localization error.[17] The localization error is defined as the square root of the variance of the distribution of position estimates. Here, the unbiased sample variance (divide by $M-1$) must be used instead of the usual sample variance (divide by M) to compensate for the bias in estimating the variance for short run lengths M. This measure for the localization error can be compared directly to the mean MLE-based localization uncertainty. The advantage of this method is that it does not require analysis of additional beads or of hand-picked clusters of localizations originating from isolated emitters.

We have analyzed a dataset (an acquisition of Alexa 647-labeled tubulin networks in fixed HeLa cells, shown in Figure 2a of ref. [28]) to compare the analytical approximation Equation (7) with the MLE-based localization uncertainty $\Delta x|_{\mathrm{MLE}}$ obtained from the numerical spot-fitting procedure, as well as to compare the root-mean-square localization error of a group of subsequent localization events $\Delta x|_{\mathrm{loc}}$ with the mean value of $\Delta x|_{\mathrm{MLE}}$ for the sequence of localizations. The average (standard deviation) of the dimensionless background parameter τ over all grouped localization events was 0.53 (0.28) and the average (standard deviation) of the ratio of the analytical approximation of the numerical MLE-based localization uncertainty $\Delta x|_{\mathrm{MLE}}$ over all grouped localization events was 1.013 (0.026), thus indicating an excellent agreement between the two descriptions. Incidentally, for this background level the difference between MLE- and LS-based fitting is only about 3%, consistent with the small difference in image resolution reported in ref. [28].

Figure 3 shows the scaled localization error as a function of the scaled background parameter together with the prediction of Equation (7), which shows excellent agreement. Figure 3 also shows the ratio of the localization error and the MLE-based localization uncertainty as a function of run length of the event. The ratio increases somewhat for larger run lengths from a value close to 1 for the shorter run lengths to a value a bit elevated above 1 for the larger run lengths. The average (weighted with the inverse variance) over all run lengths shows that the measured localization error is about 3% higher than the MLE-based localization uncertainty. It may be concluded that the MLE-based localization uncertainty $\Delta x|_{\mathrm{MLE}}$ is a good predictor of the experimental localization uncertainty. We have also investigated the effects of filtering the set of found localization events. It is custom, for example, to ignore the dimmer localization events in order to avoid false positives. Different settings of the fit parameter ranges that are deemed as acceptable can give rise to variations of a few percent in the reported ratio between the experimental and predicted localization uncertainty (data not shown).

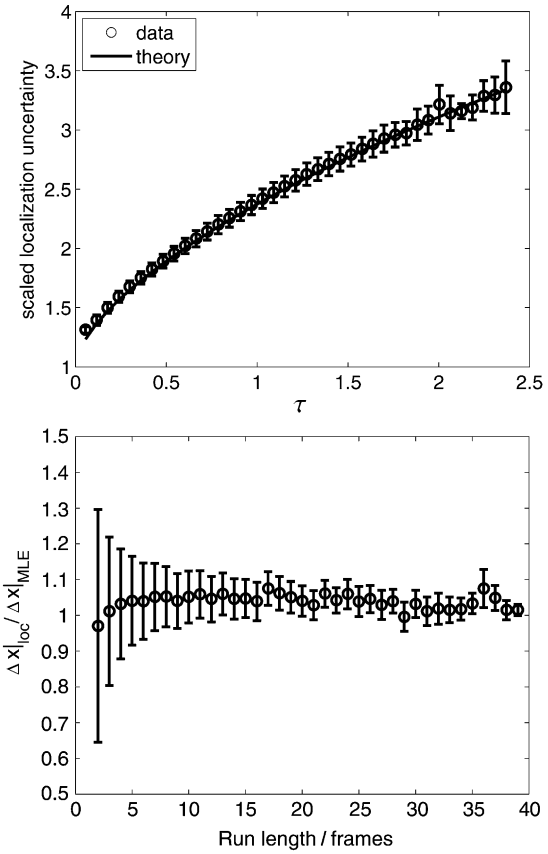

Figure 3. Measured scaled localization error $\Delta x|_{\mathrm{loc}}\sqrt{N}/\sigma$ as a function of the measured scaled background parameter τ with the theoretical curve of Equation (7) (top) showing excellent agreement between theory and experiment, and the ratio of the localization error and the mean MLE-based estimate of the localization uncertainty as a function of the run length of the group of subsequent localizations of the same emitter (bottom) showing a ratio close to 1.

2.3. Axial Localization Uncertainty

2.3.1. Bifocal Method

In the bifocal method two mutually defocused spots are measured giving estimates for the lateral position and for the spot width σ_j, the signal photon count N_j, and background photon count per pixel b_j in the two defocused channels $j=\pm$. The expected values for the spot widths are modeled by [Eq. (10)]:

$$\sigma_{\pm}^2 = \sigma_0^2\left[1+\frac{(z\pm l)^2}{d^2}\right] \qquad (10)$$

with σ_0 the spot size in focus, z the axial position of the emitter, $2l$ the mutual defocus of the two channels, and d a measure of the focal depth. Usually, both l and d are obtained by a calibration measurement. The axial emitter position can be derived most easily from the focus S curve [Eq. (11)]:

$$F = \frac{\sigma_+^2 - \sigma_-^2}{\sigma_+^2 + \sigma_-^2} = \frac{2lz}{l^2 + d^2 + z^2} \tag{11}$$

which, advantageously, does not depend on the nominal spot width σ_0 but only on the to-be-determined axial position z and on the two calibration parameters l and d. Inverting this relation gives the axial position as [Eq. (12)]:

$$z = \frac{(l^2 + d^2)F}{l + \sqrt{l^2 + (l^2 + d^2)F^2}} \tag{12}$$

The axial position can be determined uniquely from F in the range $\sqrt{l^2 + d^2} > z > -\sqrt{l^2 + d^2}$. Expanding this range requires a different procedure with knowledge of the parameter σ_0. Significant gains in axial range are not realistic, as the success rate of the fitting procedure and the lateral localization uncertainty deteriorate for the large spot sizes at axial positions beyond $\pm\sqrt{l^2 + d^2}$. This may be improved by multifocal imaging.[29,30]

The MLE-based uncertainty in $\sigma_\pm$ is given by Equation (8). Error propagation then leads to an uncertainty in F [Eq. (13)]:

$$(\Delta F)^2 = (1 - F^2)\left[\left(\frac{\Delta\sigma_+}{\sigma_+}\right)^2 + \left(\frac{\Delta\sigma_-}{\sigma_-}\right)^2\right] \tag{13}$$

and an uncertainty in z [Eq. (14); bf = bifocal]:

$$(\Delta z)^2_{\mathrm{bf}} = \frac{(l^2 + d^2 + z^2)^4}{4l^2(l^2 + d^2 - z^2)^2}(\Delta F)^2 \tag{14}$$

The axial localization uncertainty is lowest at $z = 0$ and increases towards the outer values of the defocus range $\pm\sqrt{l^2 + d^2}$. At $z = 0$ we find [Eq. (15)]:

$$(\Delta z)_{\mathrm{bf}} = \frac{l^2 + d^2}{2l\sqrt{N}}\sqrt{1 + 8\tau + \sqrt{\frac{8\tau}{1 + 2\tau}}} \tag{15}$$

in which it is also used that on average $N_+ = N_- = N/2$ and $b_+ = b_- = b/2$, with N and b the total number of signal and background photons, respectively, so that [Eq. (16)]:

$$\tau_\pm = \tau = \frac{2\pi b\left[\sigma_0^2(1 + l^2/d^2) + a^2/12\right]}{Na^2} \tag{16}$$

The lowest uncertainty is found for $l = d$ leading to a scaling proportional to $d/2\sqrt{N}$ and a background parameter $\tau = 2\pi b(2\sigma_0^2 + a^2/12)/Na^2$ that is roughly twice as large as for the nominal 2D case. The axial localization uncertainty is worse than the lateral localization uncertainty for a number of reasons. First, the depth of focus d is larger than the lateral spot width, typically by a factor of about 3. Second, the dependence on the relative background level τ has a negative impact, that is, the ratio of the localization uncertainty with background to the value without background is worse for the axial case than for the lateral case. Finally, the defocus makes the spot size larger and hence the signal-to-background ratio is also worse than for the nominal 2D case. This effect influences both the lateral and axial localization uncertainty in a negative way.

2.3.2. Astigmatic Method

The conclusions for the astigmatic method are largely the same as for the bifocal method. Now the spot widths in x and y are given by [Eq. (17)]:

$$\sigma_\pm^2 = \sigma_0^2\left[1 + \frac{(z \pm l)^2}{d^2}\right] \tag{17}$$

with σ_0 the spot size in focus, z the axial position of the emitter, $2l$ the distance between the focal lines, and d a measure of the focal depth. Clearly, the analysis for the bifocal method can be adapted to the astigmatic case easily. The only difference that arises is in the MLE-based uncertainty for the spot widths in x and y, which is slightly different from the bifocal case (see the Supporting Information for a derivation). For $z = 0$ we now find [Eq. (18); as = astigmatic]:

$$(\Delta z)_{\mathrm{as}} = \frac{l^2 + d^2}{2l\sqrt{N}}\sqrt{1 + 8\tau + \sqrt{\frac{9\tau}{1 + 4\tau}}} \tag{18}$$

which differs from the bifocal case only in the last term under the square root.

2.3.3. Double-Helix Method

The double-helix spot can be modeled by a bi-Gaussian PSF with lateral positions at [Eqs. (19) and (20)]:

$$x_\pm = x_0 \pm h\cos(\pi z/2l) \tag{19}$$

$$y_\pm = y_0 \pm h\sin(\pi z/2l) \tag{20}$$

in which h is the distance between the two spots and $l > z > -l$ defines the axial range. The axial position of the emitter is then given by [Eq. (21)]:

$$z = \frac{2l}{\pi}\arctan\left(\frac{y_+ - y_-}{x_+ - x_-}\right) \tag{21}$$

In each of the two subspots typically half of the signal photons are captured, thereby deteriorating the localization uncertainty by a factor of $\sqrt{2}$. In addition, the local signal-to-background ratio is also decreased by a factor of 2, which makes the local background parameter τ twice as large as the case in which all signal energy is focused into a single spot. The uncertainty in $x_\pm$ (and $y_\pm$) is therefore given by a modification of Equation (7) ($N \to N/2$, $\tau \to 2\tau$) [Eq. (22)]:

$$\Delta x_\pm|^2_{\mathrm{MLE}} = \frac{2(\sigma^2 + a^2/12)}{N}\left(1 + 8\tau + \sqrt{\frac{4\tau}{1 + 8\tau}}\right) \tag{22}$$

Error propagation then gives the uncertainty for the axial position as [Eq. (23); dh = double helix]:

$$(\Delta z)_{dh} = \frac{l\sqrt{\sigma^2 + a^2/12}}{\pi h\sqrt{N}}\sqrt{1 + 8\tau + \sqrt{\frac{4\tau}{1+8\tau}}} \quad (23)$$

The double-helix method allows for more degrees of freedom in the optical design, characterized by the parameters l, σ, and h, than the bifocal or astigmatic methods. This additional freedom can be used to engineer an optimum compromise between the axial range l, the lateral localization uncertainty, and the axial localization uncertainty.[17] The dependence on the background parameter τ, however, is not that different from the bifocal or astigmatic methods. The same conclusions on the quality of axial localization compared to lateral localization thus also hold here. Figure 4 shows a plot of the relative

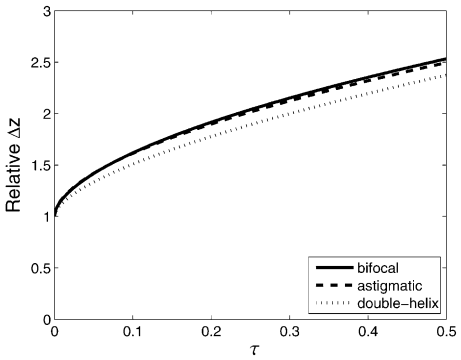

Figure 4. Dependence of the axial localization uncertainty on the background parameter τ relative to the uncertainty at zero background for the bifocal, astigmatic, and double-helix methods, which shows a similar dependence for all three methods.

increase in axial localization uncertainty with background compared to the value for zero background, in which it is assumed that the in-focus spot sizes for the bifocal and astigmatic methods are equal to the spot size of the double-helix method. All three methods show a similar dependence on background but the double-helix method is slightly better than the other two. This largely agrees with previous findings.[17,21–24]

3. Conclusions

We have demonstrated that three measures for the lateral localization uncertainty substantially coincide: the CRLB of the MLE fitting procedure, a concise analytical approximation to the CRLB, depending only on spot width and signal and background photon count, and the experimental localization error obtained from analyzing single-molecule activation events with run lengths of multiple image frames. All measures are in mutual agreement within a few percent error.

The increase of the localization uncertainty by a factor of $\sqrt{2}$ due to the excess noise of the EM-CCD cannot be distinguished from an underestimation of the photon count by a factor of 2 with current image analysis protocols for calibrating the camera gain. This does not imply that the negative effect of excess noise on the localization uncertainty is not present. In fact, recently two different methods have been proposed that deal with this problem. Chao et al.[31] spread out the image of a single emitter over a large area, thus lowering the photon count per pixel to a level at which the excess noise is negligible. Huang et al.[32] use scientific complementary metal oxide–semiconductor (sCMOS) cameras, which have no excess noise and a very low readout noise and a high frame rate, and show that gains in localization uncertainty as well as image acquisition speed can be achieved.

We have also generalized the approach for deriving an analytical approximation to the lateral localization uncertainty to the case of axial localization. Closed-form expressions for the axial localization uncertainty for the bifocal, astigmatic, and double-helix methods are presented. It appears that the axial localization uncertainty is worse than the lateral localization uncertainty not only because of the difference between the axial and lateral spot sizes, but also because of a more unfavorable dependence on background level. This background dependence is largely the same for the three methods. In addition, the more spread-out spots relative to standard 2D localization induce a lower signal-to-background ratio, thus giving an overall lower localization uncertainty both in lateral and axial directions.

Possible next steps in analyzing and improving performance limits are related to methods that deal with raw images that are less sparse than for the standard way of operation, for example, methods for fitting multiple emitters in one ROI.[33,34] It is mentioned that not all of these methods can be characterized in a straightforward fashion by a quantitative performance measure such as the localization uncertainty.[35–38]

Acknowledgements

We thank Robert Nieuwenhuizen for help in analyzing the datasets of ref. [28] and Keith Lidke for providing a software template in C for grouping spatially nearby localizations in subsequent image frames.

Keywords: analytical approximations · localization microscopy · maximum likelihood estimation · single-molecule studies · super-resolution light microscopy

[1] E. Betzig, G. H. Patterson, R. Sougrat, O. W. Lindwasser, S. Olenych, J. S. Bonifacino, M. W. Davidson, J. Lippincott-Schwartz, H. F. Hess, *Science* **2006**, *313*, 1642 – 1645.
[2] S. T. Hess, T. P. Girirajan, M. D. Mason, *Biophys. J.* **2006**, *91*, 4258 – 4272.
[3] M. J. Rust, M. Bates, X. Zhuang, *Nat. Methods* **2006**, *3*, 793 – 795.
[4] J. Fölling, M. Bossi, H. Bock, R. Medda, C. A. Wurm, B. Hein, S. Jakobs, C. Eggeling, S. W. Hell, *Nat. Methods* **2008**, *5*, 943 – 945.
[5] M. Heilemann, S. van de Linde, M. Schüttpelz, R. Kasper, B. Seefeldt, A. Mukherjee, P. Tinnefeld, M. Sauer, *Angew. Chem.* **2008**, *120*, 6266 – 6271; *Angew. Chem. Int. Ed.* **2008**, *47*, 6172 – 6176.
[6] S. Stallinga, B. Rieger, *Opt. Express* **2010**, *18*, 24461 – 24476.

[7] R. E. Thompson, D. R. Larson, W. W. Webb, *Biophys. J.* **2002**, *82*, 2775 – 2783.
[8] K. I. Mortensen, L. S. Churchman, J. A. Spudich, H. Flyvbjerg, *Nat. Methods* **2010**, *7*, 377 – 384.
[9] R. J. Ober, S. Ram, S. E. Ward, *Biophys. J.* **2004**, *86*, 1185 – 1200.
[10] A. V. Abraham, S. Ram, J. Chao, E. S. Ward, R. J. Ober, *Opt. Express* **2009**, *17*, 23352 – 23373.
[11] S. Stallinga, B. Rieger, *IEEE Int. Symp. Biomed. Imaging* **2012**, 988 – 991.
[12] C. S. Smith, N. Joseph, B. Rieger, K. A. Lidke, *Nat. Methods* **2010**, *7*, 373 – 375.
[13] M. Bates, G. T. Dempsey, K. H. Chen, X. Zhuang, *ChemPhysChem* **2012**, *13*, 99 – 107.
[14] B. Huang, W. Wang, M. Bates, X. Zhuang, *Science* **2008**, *319*, 810 – 813.
[15] M. F. Juette, T. J. Gould, M. D. Lessard, M. J. Mlodzianoski, B. S. Nagpure, B. T. Bennett, S. T. Hess, J. Bewersdorf, *Nat. Methods* **2008**, *5*, 527 – 530.
[16] S. R. P. Pavani, R. Piestun, *Opt. Express* **2008**, *16*, 22048 – 22057.
[17] G. Grover, K. DeLuca, S. Quirin, J. DeLuca, R. Piestun, *Opt. Express* **2012**, *20*, 26681 – 26695.
[18] C. Bricot, J. C. Lehureau, C. Puech, F. Le Carvennec, *IEEE Trans. Consum. Electron.* **1976**, *CE-22*, 304 – 308.
[19] D. K. Cohen, W. H. Gee, M. Ludeke, J. Lewkowicz, *Appl. Opt.* **1984**, *23*, 565 – 570.
[20] M. S. Wang, T. D. Milster, *Appl. Opt.* **1993**, *32*, 4797 – 4807.
[21] C. von Middendorff, A. Egner, C. Geisler, S. W. Hell, A. Schönle, *Opt. Express* **2008**, *16*, 20774 – 20788.
[22] M. J. Mlodzianoski, M. F. Juette, G. L. Beane, J. Bewersdorf, *Opt. Express* **2009**, *17*, 8264 – 8277.
[23] G. Grover, S. R. P. Pavani, R. Piestun, *Opt. Lett.* **2010**, *35*, 3306 – 3308.
[24] M. Badieirostami, M. D. Lew, M. A. Thompson, W. E. Moerner, *Appl. Phys. Lett.* **2010**, *97*, 161103.
[25] J. Hynecek, T. Nishiwaki, *IEEE Trans. Electron Devices* **2003**, *50*, 239 – 245.
[26] J. Chao, E. S. Ward, R. J. Ober, *Multidimens. Syst. Signal Process.* **2012**, *23*, 349 – 379.
[27] J. C. Mullikin, L. J. van Vliet, H. Netten, F. R. Boddeke, G. van der Feltz, I. T. Young, *Proc. SPIE* **1994**, *2173*, 73 – 84.
[28] R. P. J. Nieuwenhuizen, K. A. Lidke, M. Bates, D. Leyton Puig, D. Grünwald, S. Stallinga, B. Rieger, *Nat. Methods* **2013**, *10*, 557 – 562.
[29] S. Ram, P. Prabhar, J. Chao, E. S. Ward, R. J. Ober, *Biophys. J.* **2008**, *95*, 6025 – 6043.
[30] S. Abrahamsson, J. Chen, B. Hajj, S. Stallinga, A. Y. Katsov, J. Wisniewski, G. Mizuguchi, P. Soule, F. Mueller, C. D. Darzacq, X. Darzacq, C. Wu, C. I. Bargmann, D. A. Agard, M. Dahan, M. G. L. Gustafsson, *Nat. Methods* **2013**, *10*, 60 – 63.
[31] J. Chao, S. Ram, E. S. Ward, R. J. Ober, *Nat. Methods* **2013**, *10*, 335 – 338.
[32] F. Huang, T. M. P. Hartwich, F. E. Rivera-Molina, Y. Lin, W. C. Duim, J. J. Long, P. D. Uchil, J. R. Myers, M. A. Baird, W. Mothes, M. W. Davidson, D. Toomre, J. Bewersdorf, *Nat. Methods* **2013**, *10*, 653 – 658.
[33] S. J. Holden, S. Uphoff, A. N. Kapanidis, *Nat. Methods* **2011**, *8*, 279 – 280.
[34] F. Huang, S. L. Schwartz, J. M. Byars, K. A. Lidke, *Biomed. Opt. Express* **2011**, *2*, 1377 – 1393.
[35] T. Dertinger, R. Colyer, G. Iyer, S. Weiss, J. Enderlein, *Proc. Natl. Acad. Sci. USA* **2009**, *106*, 22287 – 22292.
[36] T. Quan, H. Zhu, X. Liu, Y. Liu, J. Ding, S. Zeng, Z.-L. Huang, *Opt. Express* **2011**, *19*, 16963 – 16974.
[37] L. Zhu, W. Zhang, D. Elnatan, B. Huang, *Nat. Methods* **2012**, *9*, 721 – 726.
[38] E. A. Mukamel, H. Babcock, X. Zhuang, *Biophys. J.* **2012**, *102*, 2391 – 2400.

Received: August 1, 2013
Revised: October 24, 2013
Published online on December 2, 2013